Mathematical Biosciences and Engineering

MBE, 16(5): 5640–5651
DOI: 10.3934/mbe.2019280
Received: 10 February 2019
Accepted: 30 May 2019
Published: 18 June 2019

http://www.aimspress.com/journal/MBE

Research article

Impact of region of interest size on transcranial sonography based computer-aided diagnosis for Parkinson's disease

Xiaoyan Fei [1], Yun Dong [2], Hedi An [3], Qi Zhang [1], Yingchun Zhang [4] and Jun Shi [1,*]

[1] Key Laboratory of Specialty Fiber Optics and Optical Access Networks, Shanghai Institute for Advanced Communication and Data Science, School of Communication and Information Engineering, Shanghai University, Shanghai, China
[2] Department of Ultrasonography, Shanghai East Hospital of Tongji University, Shanghai, China
[3] Department of Neurology, Shanghai East Hospital of Tongji University, Shanghai, China
[4] Department of Ultrasound, The Second Affiliated Hospital of Soochow University, China

* **Correspondence:** Email: junshi@shu.edu.cn; Tel: +86-21-66137269.

Abstract: Transcranial sonography (TCS) has gained increasing application for diagnosis of Parkinson's disease (PD) in clinical practice in recent years, because most PD patients, even in the early stage of PD, have abnormal hyperechogenicity of the substantia nigra (SN) in brainstem shown in TCS images. Therefore, the region of interest (ROI) for feature extraction should cover the SN region in a computer-aided diagnosis (CAD) system. The ROI size naturally affects the feature representation. However, there currently exist no unified standard for determining the size of ROI. In this work, we quantitatively compare the performance of TCS-based CAD with three sizes of ROIs, namely the entire midbrain (EM) region, the half of midbrain (HoM) region and the SN region. The experimental results on the original extracted features and the features by dimensionality reduction show that ROI covering the EM region achieves the overall best diagnosis performance. The results indicates that the neighboring regions around SN might also have abnormal symptoms, which cannot be clearly observed with naked eyes. It suggests that the large ROI includes more information for feature representation to improve the diagnosis performance of TCS-based CAD for PD.

Keywords: Parkinson's disease; transcranial sonography; region of interest; substantia nigra

1. Introduction

Parkinson's disease (PD) is the second most common degenerative disorder of the central nervous system after Alzheimer's disease in the elderly population worldwide [1,2]. PD not only immensely affects the patient's quality of life, but also results in a high socioeconomic burden.

Early and accurate diagnosis of PD is crucial for early intervention and neuroprotective strategies to delay or prevent the progression of PD. However, PD diagnosis mainly depends on the patient's clinical symptoms together with the expertise of the clinical neurologist, and thus has high possibility of missed diagnosis and misdiagnosis due to the complexity of PD [3].

Neuroimaging techniques, such as magnetic resonance imaging (MRI), functional MRI (fMRI), positron emission tomography (PET) and single photon emission tomography (SPECT), have shown their effectiveness in facilitating early and even preclinical diagnosis for PD [2,3].

Transcranial sonography (TCS) is a valid neuroimaging tool with the advantages of high mobility, non-invasiveness, non-ionizing radiation and low cost. TCS can generate high-resolution B-mode images of the deep brain structure parenchyma through the intact skull. In recent years, TCS has gained increasing application in diagnosis of PD [3,4], because most PD patients, even in the early stage of PD, have abnormal hyperechogenicity of the substantia nigra (SN) in brainstem shown in TCS images [3,4].

On the other hand, since the ultrasound-based computer-aided diagnosis (CAD) systems have shown the effectiveness to offer effective decision support and a second opinion tool for sonologists for diagnosis of various tumors [5–8], various TCS-based CADs for PD have also been proposed in recent years. For example, Chen et al. proposed a 2D-TCS-based CAD for PD that adopted the local features to represent the properties of the SN region [9]; Pauly et al. proposed to detect SN region from 3D TCS images with random forests [10]; Plate et al. reported a 3D-TCS image-based CAD for PD using the support vector machine (SVM) classifier [11]; Sakalauskas et al. proposed a semi-automated segmentation algorithm to segment the midbrain region in TCS images for further analysis [12], and they further developed a CAD system for PD [13]; Gong et al. proposed a deep neural mapping large margin distribution machine for TCS-based diagnosis PD [14]; Shi et al. developed a cascaded multi-column RVLF+ classifier algorithm and then applied it to the TCS-based CAD for PD [15]. All these studies indicate feasibility and effectiveness of TCS-based CAD for PD.

However, it is worth noting that no unified standard is proposed to select the region of interest (ROI) in TCS images for feature extraction in current research. The commonly used ROIs only include the SN region or a region that is slightly larger than SN [11], such as the half of midbrain (HoM) region [9]. In fact, the size of ROI naturally affects the representation of extracted features [16,17]. However, no studies exist on quantitative analysis of this impact on the diagnosis performance of TCS-based CAD for PD.

In this work, we quantitatively evaluate the impact of three sizes of ROIs, namely the entire midbrain (EM) region, the HoM region and the SN region, on the diagnosis performance of the TCS-based CAD for PD.

2. Materials and method

2.1. TCS datasets

The TCS dataset includes 153 images (76 PD patients and 77 normal controls (NCs)), which were acquired from the Shanghai East Hospital of Tongji University and the Second Affiliated Hospital of Soochow University was used in this work. The approval from the ethics committee of the hospital was obtained, and all subjects had signed informed consent.

The TCS images from the Shanghai East Hospital of Tongji University were scanned by a Philips IE33 color ultrasound scanner (Philips Healthcare, Bothell, Washington, USA) with a S5-1 phased array probe (Philips Healthcare, Bothell, Washington, USA). The data from the Second Affiliated Hospital of Soochow University were acquired by a Siemens Acuson Sequoia 512 ultrasound scanner (Siemens Medical Solutions, Malvern, Pennsylvania, USA) with a 4V1C prober (Siemens Medical Solutions, Malvern, Pennsylvania, USA). The probe frequency was set to 2–3 MHz, the penetration depth is 13–16 cm, and the dynamic range is 45–60 dB in both hospitals. Other imaging parameters, such as gain and time-gain compensation, were set for clear visualization of each subject. After the subject was positioned on the bed, the TCS images were scanned through the right or left temporal bone windows in the axial plane. For each subject, one TCS image was selected for further analysis.

Since the abnormal hyperechogenicity of the SN in brainstem is a typical sign of PD found in TCS images [3,4], the ROI should include the SN in each TCS image. After all the TCS images were acquired from the two hospitals, the ROIs were manually selected by an experienced sonologist from the Shanghai East Hospital of Tongji University, which can help to reduce the impact of ROI selection by different sonologists to a certain extent. Figure 1 shows the example ROIs of the EM, HoM and SN regions from TCS images of a PD patient and an NC, respectively.

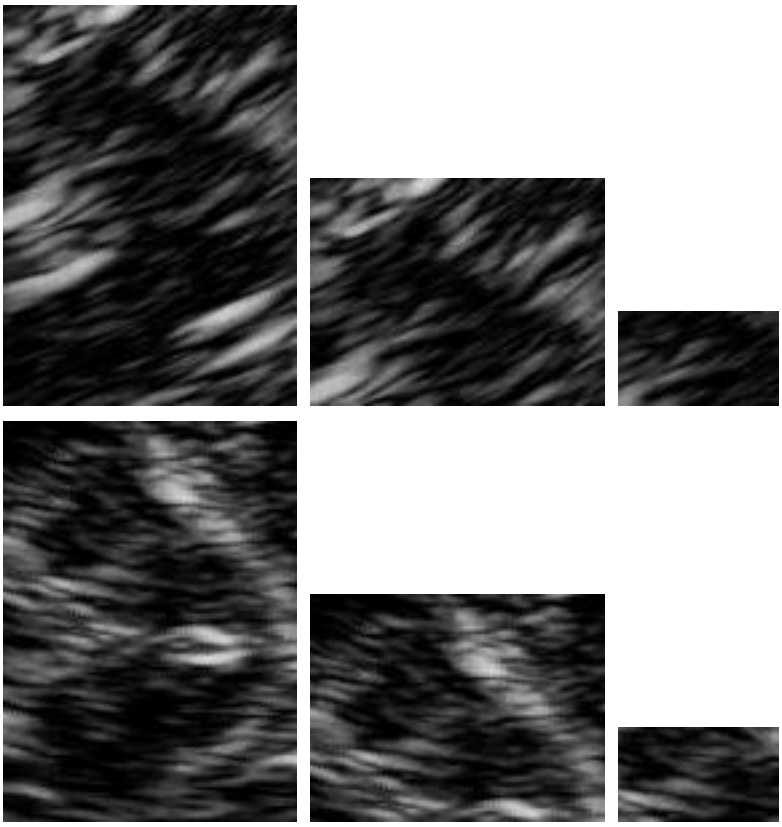

Figure 1. Example ROIs of the EM, HoM and SN in TCS images (from left to right) from an NC (first row) and a PD patient (second row).

2.2. TCS-based CAD for PD

Figure 2 shows the flowcharts for PD diagnosis by the TCS-based CAD, which mainly includes the modules of feature extraction, dimensionality reduction and classifier.

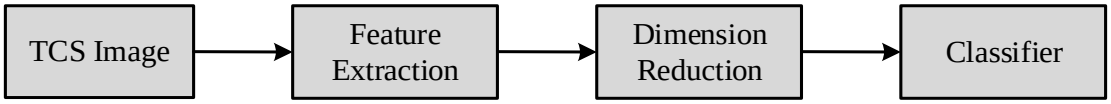

Figure 2. Flowchart of the TCS-based CAD.

For the TCS images, the statistical features and texture features were directly extracted from each ROI in this work. The statistical features were calculated from the intensities of all pixels in ROI, including the mean, standard deviation, coefficient of variance, skewness, kurtosis, entropy of histogram, area ratio, combined area ratio, and several percentiles, etc. Additional details of these features can be found in reference [18]. The texture features were extracted from the gray-level co-occurrence matrix (GLCM), including the energy, contrast, homogeneity and entropy of GLCM. Moreover, the features of Hu invariant moments were also extracted according to reference [9]. We subsequently obtained 73-dimensional features in total from each TCS image. It is worth noting that to evaluate the impact of ROI size for TCS-based CAD, we selected three sizes of ROIs according to the anatomic information in this work, including the EM region, the HoM region and only the SN region, respectively. The same features were then extracted for different sizes of ROIs.

In this work, the dimensionality reduction algorithms were also performed on the original features to generate compact feature representation that could more comprehensively evaluate the performance of different size ROIs in TCS images. Although many dimensionality reduction algorithms have been proposed [19–22], we selected the classical principal component analysis (PCA) and minimum redundancy maximum relevance (MRMR) [23] to reduce feature redundancy, respectively. Since both algorithms are widely used in dimensionality reduction for various data, we do not repeat them here.

Since the SVM classifier has proven its effectiveness for TCS-based CAD for PD [9,11], it is also used in this work.

2.3. Experimental design

Two experiments were conducted for the TCS-based CAD. The first experiment primarily evaluated the effect of three sizes of ROIs in TCS images for diagnosis of PD, i.e. the EM region, the HoM region and only the SN region, respectively. The same 73-dimensional features were extracted from these three sizes of ROIs. The second one conducted the widely used PCA and MRMR on the original features to reduce the feature dimensionalities of the original features for further comprehensive comparison. Therefore, in total, three types of features were extracted for each size of ROIs. The extracted features were subsequently fed to the SVM classifier in the first experiment.

The 5-fold cross-validation strategy was performed on the single-modal TCS dataset with 153 subjects to avoid the sampling bias introduced by randomly partitioning the dataset in cross-validation. The classification accuracy (Acc), sensitivity (Sen), specificity (Spe), Youden index

(YI), positive predictive value (PPV), negative predictive value (NPV) and F1-score were calculated as evaluation indices by

$$\begin{cases} Acc = (TP + TN)/(FP + FN + TN + FP) \\ Sen = TP/(TP + FN) \\ Spe = TN/(TN + FP) \\ YI = Sen + Spe - 1 \\ PPV = TP/(TP + FP) \\ NPV = TN/(TN + FN) \\ F1 = 2 \times PPV \times Sen/(PPV + Sen) \end{cases} \tag{11}$$

where TP, FP, FN and TN are true positive, false positive, false negative and true negative, respectively.

3. Results

Table 1 shows the results of TCS-based CADs of three ROIs with the commonly used linear kernel SVM on the original features. It can be found that the EM-based diagnosis achieves the overall best results with the best mean accuracy of 75.16 ± 1.77%, sensitivity of 79.67 ± 5.10%, YI of 49.92 ± 4.89%, PPV of 71.55 ± 8.97%, NPV of 77.03 ± 9.62%, F1-score of 73.96 ± 4.65%, and the second best specificity of 70.25 ± 6.70%. Moreover, the overall performance of the HoM-based method is also superior to that of the SN-based approach, and obtains the best mean specificity of 74.08 ± 9.99% and the second best mean accuracy of 73.25 ± 4.53%, sensitivity of 72.36 ± 9.68%, YI of 46.44 ± 9.05%, PPV of 71.00 ± 6.38% NPV of 73.63 ± 6.87% and F1-score of 72.73 ± 4.93%.

Table 1. Results of TCS-based CAD for three sizes of ROIs with linear kernel SVM on the original features. (Unit: %)

	Accuracy	**Sensitivity**	**Specificity**	**YI**	**PPV**	**NPV**	**F1**
SN	70.80 ± 4.42	61.52 ± 8.43	69.45 ± 6.32	30.97 ± 8.58	70.74 ± 5.70	69.15 ± 4.79	70.90 ± 4.96
HoM	73.25 ± 4.53	72.36 ± 9.68	**74.08 ± 9.99**	46.44 ± 9.05	71.00 ± 6.38	73.63 ± 6.87	72.73 ± 4.93
EM	**75.16 ± 1.77**	**79.67 ± 5.10**	70.25 ± 6.70	**49.92 ± 4.89**	**71.55 ± 8.97**	**77.03 ± 9.62**	**73.96 ± 4.65**

Table 2 gives the results of TCS-based CADs of three ROIs with the commonly used Gaussian kernel SVM on the original features. The EM-based method again achieves the overall best performance with the best mean accuracy, sensitivity, specificity, YI, PPV, NPV and F1-value of 71.85 ± 4.11%, 73.52 ± 7.24%, 70.17 ± 9.90%, 43.69 ± 8.44%, 71.31 ± 7.99%, 73.25 ± 3.08% and 71.33 ± 4.44%, respectively. The overall results of the HoM-based diagnosis are next to those of the EM-based one, obtaining the second best mean accuracy, sensitivity, specificity, YI, PPV, and F1-score of 70.56 ± 4.85%, 72.08 ± 6.33%, 69.08 ± 9.53%, 41.16 ± 9.98%, 70.01 ± 8.01%, 71.78 ± 3.27% and 70.86 ± 5.17%, respectively. Tables I and II show consistent results, suggesting that the larger ROIs can promote diagnosis performance compared with the SN region.

Table 2. Results of TCS-based CAD for three sizes of ROIs with Gaussian kernel SVM on the original features. (Unit: %)

	Accuracy	Sensitivity	Specificity	YI	PPV	NPV	F1
SN	69.31 ± 2.45	71.12 ± 4.98	67.50 ± 6.56	38.62 ± 4.78	68.60 ± 2.95	70.36 ± 3.78	69.68 ± 1.97
HoM	70.56 ± 4.85	72.08 ± 6.33	69.08 ± 9.53	41.16 ± 9.98	70.01 ± 8.01	71.78 ± 3.27	70.86 ± 5.17
EM	**71.85 ± 4.11**	**73.52 ± 7.24**	**70.17 ± 9.90**	**43.69 ± 8.44**	**71.31 ± 7.99**	**73.25 ± 3.08**	**71.33 ± 4.44**

Figure 3 shows the compared results of different dimensional features for three sizes of ROIs, where the features are reduced by the conventional PCA algorithms. In this experiment, we only adopted the linear kernel SVM as classifier, because it achieved performance superior to the Gaussian kernel SVM. Moreover, we only give the results of YI, since it is a hybrid index combining both sensitivity and specificity. It can be found that both the EM- and HoM-based diagnosis outperform the SN-based classification for different feature dimensionalities. Moreover, the EM-based option achieves the overall best performance with the best classification accuracy, specificity, YI and PPV, whereas the HoM-based classification obtains the best sensitivity, NPV and F1-score.

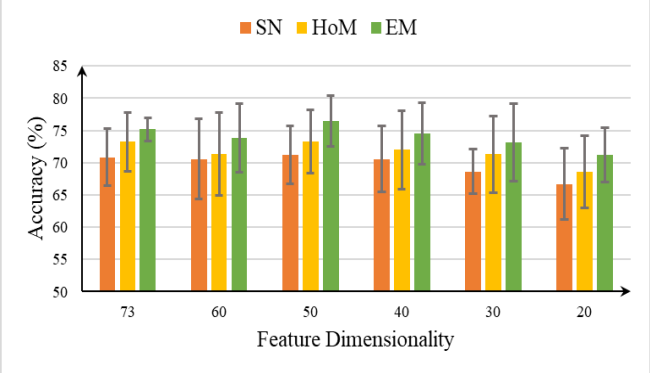

(a)

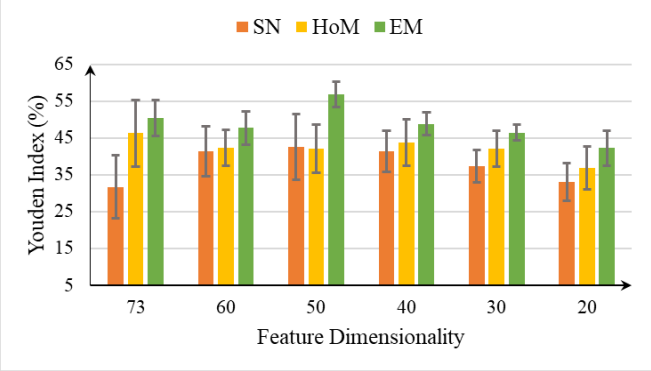

(b)

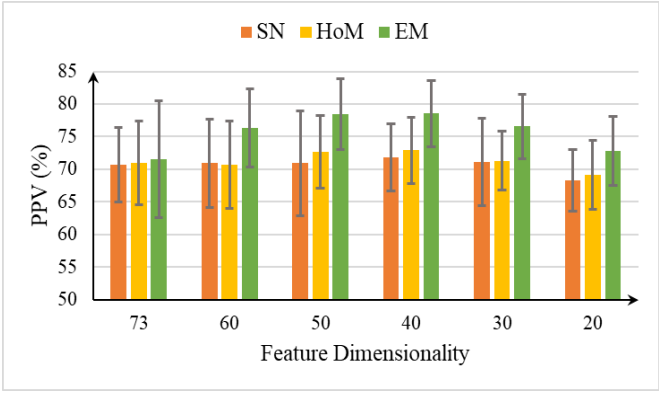

(c)

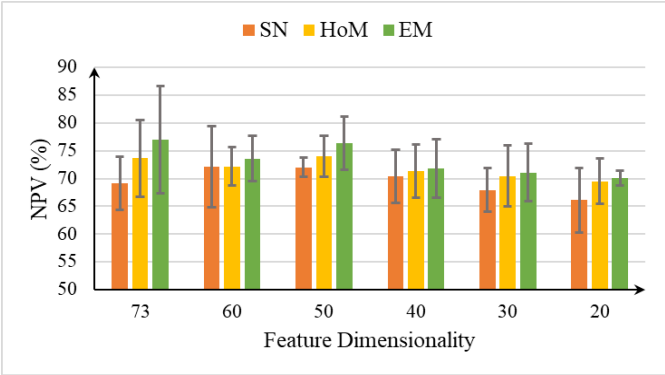

(d)

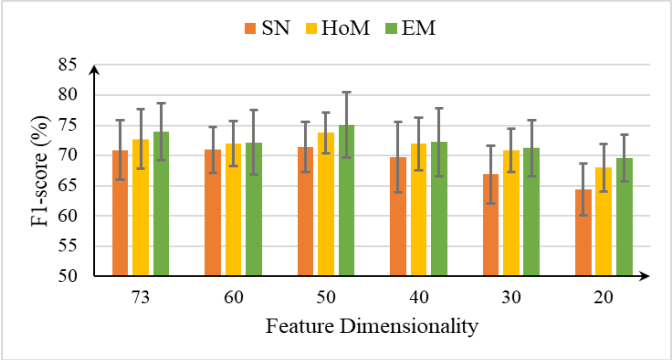

(e)

Figure 3. Results of (a) classification accuracy, (b) YI, (c) PPV, (d) NPV and (e) F1-score for different dimensional features by PCA for EM-, HoM- and SN-based CAD.

Figure 4 gives the compared results of different dimensional features for three sizes of ROIs, where the features are selected by the conventional MRMR algorithm. Again the linear kernel SVM is used in this experiment. The results show trends similar to those in Figure 3. Both EM- and HoM-based CAD are superior to the SN-based approach, and the EM-based diagnosis achieves the best overall performance on all evaluation indices.

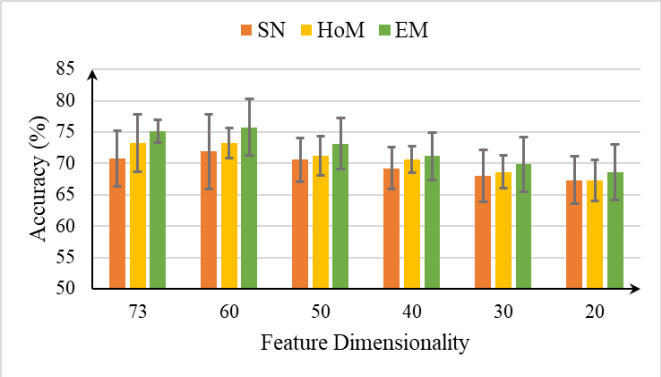
SN
HoM
EM
Accuracy (%)
85
80
75
70
65
60
55
50
73
60
50
40
30
20
Feature Dimensionality

(a)

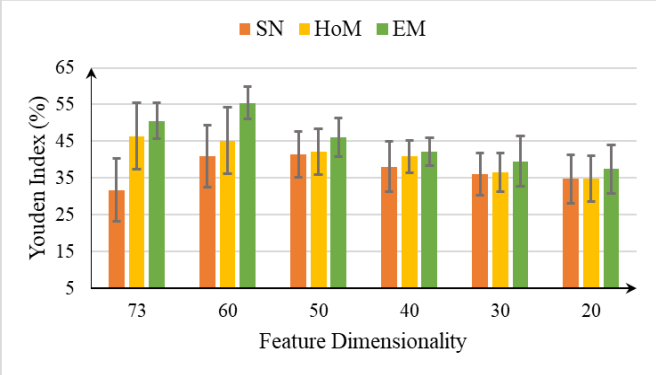
SN
HoM
EM
Youden Index (%)
65
55
45
35
25
15
5
73
60
50
40
30
20
Feature Dimensionality

(b)

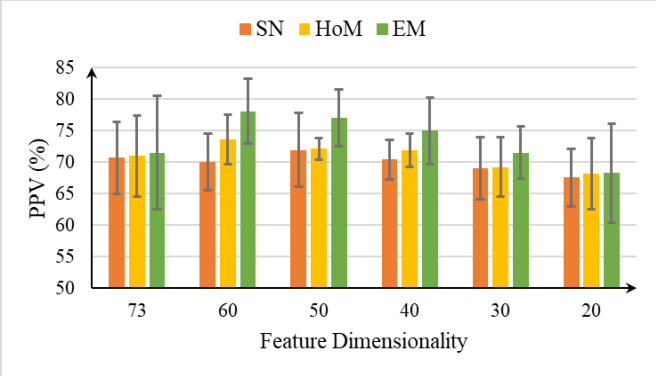
SN
HoM
EM
PPV (%)
85
80
75
70
65
60
55
50
73
60
50
40
30
20
Feature Dimensionality

(c)

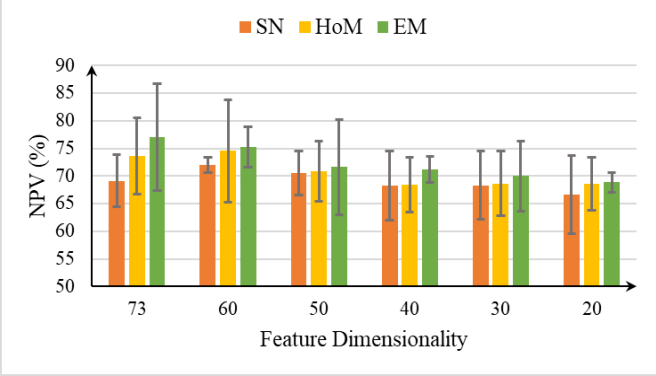
SN
HoM
EM
NPV (%)
90
85
80
75
70
65
60
55
50
73
60
50
40
30
20
Feature Dimensionality

(d)

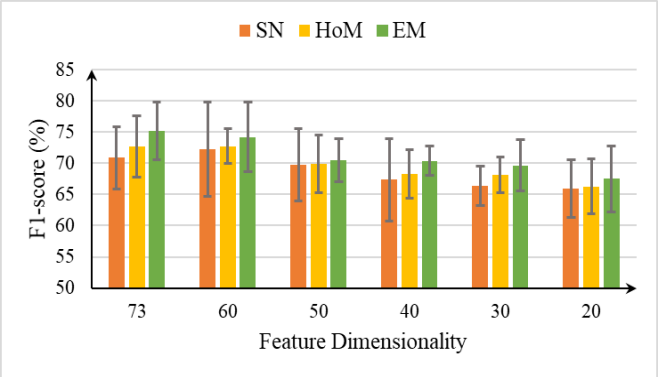

(e)

Figure 4. Results of (a) classification accuracy, (b) YI, (c) PPV, (d) NPV and (e) F1-score for different dimensional features by MRMR for EM-, HoM- and SN-based CAD.

Finally, we select the classification results of the 50-dimensional features via PCA and the 60-dimensional features by MRMR for comparison of the three sizes of ROIs, as shown in Table 3. It can be found that both EM- and HoM-based diagnosis outperform the SN-based approach with not only the original features but also the reduced features. Moreover, both PCA and MRMR can improve the performance of feature representation for all three sizes of ROIs. The EM-based classification with the features reduced by PCA achieves the overall best results with the best mean classification accuracy of 76.43 ± 3.91%, specificity of 80.58 ± 4.16%, YI of 56.97 ± 3.49%, PPV of 78.48 ± 5.46% and F1-score of 75.05 ± 5.38%, and the second best mean sensitivity of 76.39 ± 3.50% and NPV of 76.39 ± 4.74%.

Table 3. Results of TCS-based CAD for three sizes of ROIs with different dimensional features. (Unit: %)

	Accuracy	**Sensitivity**	**Specificity**	**YI**	**PPV**	**NPV**	**F1**
SN	70.80 ± 4.42	61.52 ± 8.43	69.45 ± 6.32	30.97 ± 8.58	70.74 ± 5.70	69.15 ± 4.79	70.90 ± 4.96
SN-PCA	71.89 ± 5.92	66.94 ± 5.56	74.00 ±6.53	40.94 ± 8.48	70.04 ± 4.55	72.01 ± 1.38	72.23 ± 7.57
SN-MRMR	71.20 ± 4.52	72.37 ± 2.39	70.33 ± 8.99	42.70 ± 8.93	70.91 ± 7.99	71.97 ± 1.73	71.43 ± 4.17
HoM	73.25 ± 4.53	72.36 ± 9.68	74.08 ± 9.99	46.44 ± 9.05	71.00 ± 6.38	73.63 ± 6.87	72.73 ± 4.93
HoM-PCA	73.27 ± 4.95	70.94 ± 6.44	71.33 ± 9.09	42.27 ± 6.55	72.63 ± 5.60	74.01 ± 3.71	73.74 ± 3.41
HoM-MRMR	73.23 ± 2.40	76.30 ± 9.65	68.83 ± 2.72	45.13 ± 9.03	73.58 ± 3.91	74.53 ± 9.21	72.76 ± 2.75
EM	75.16 ± 1.77	**79.67 ± 5.10**	70.25 ± 6.70	49.92 ± 4.89	71.55 ±8.97	**77.03 ± 9.62**	73.96 ± 4.65
EM-PCA	**76.43 ± 3.91**	76.39 ± 3.50	**80.58 ± 4.16**	**56.97 ± 3.49**	**78.48 ± 5.46**	76.39 ± 4.74	**75.05 ± 5.38**
EM-MRMR	75.78 ± 4.54	74.87 ± 3.78	80.56 ± 3.16	55.43 ± 5.39	78.10 ± 5.18	75.20 ± 3.69	74.24 ± 5.64

4. Discussion

With the increasing application of TCS for diagnosis of PD in clinical practice, the TCS-based CAD has also attracted considerable attention. The TCS-based diagnosis of PD mainly depends on the clinical finding that PD patients have abnormal hyperechogenicity of SN in the TCS images [3,4]. Therefore, the ROI for feature extraction should cover the SN region. The ROI size naturally affects the feature representation and the final classification performance. However, to the best of our knowledge, there currently exist no unified standard for determining the size of ROI. Therefore, we quantitatively compare the performance of TCS-based CAD with the three sizes of ROIs, namely the EM, the HoM and the SN regions in this work.

As shown in Tables 1 and 2, the EM-based CAD achieves the overall best performance by both the linear and Gaussian kernel-based SVM classifiers with the original features, whereas the HoM-based CAD is also superior to SN-based approach. Moreover, Figures 3 and 4 shows the compared results about the features reduced by both PCA and MRMR with linear SVM for different ROIs, which show the same trend with those in Table 1 and 2. All the results suggest that the large ROI-based CAD outperforms the only SN region based one. Although the SN region shows abnormal hyperechogenicity for PD patients, the neighboring regions around SN might also have abnormal symptoms, which cannot be clearly observed with naked eyes. However, the larger ROIs truly include more information, which is effectively extracted and represented by the machine learning based methods.

Since the EM-based CAD achieves the best performance, we will further develop the TCS-based CAD with EM ROI in future. In this work, we only extracted the statistical and texture features from ROI. More kinds of features, such as wavelet-based features, will be extracted to further improve the performance of CAD. Moreover, due to the success of deep learning for feature representation, we will study the deep learning algorithms for the TCS-based CAD for PD with the small sample dataset.

5. Conclusion

In summary, we quantitatively compare the impact of ROI size in TCS image on the performance of TCS-based CAD of PD. The experimental results show that the ROI covering the EM region achieves the overall best diagnosis accuracy, which will guide the selection of ROI from TCS images in future work.

Acknowledgments

This work is supported by the National Natural Science Foundation of China (61471231, 81830058, 81627804), Shanghai Science and Technology Foundation (18010500600, 17411953400, 18010500600), and the Pre-Research Project of The Second Affiliated Hospital of Soochow University (SDFEYGJ1709).

Conflict of interest

There is no conflict of interest.

References

1. R. E. Burke and O. K. Malley, Axon degeneration in Parkinson's disease. *Exp. Neurol.*, **246**(2013), 72–83.
2. C. Weingarten, M. Sundman, P. Hickey, et al., Neuroimaging of Parkinson's disease: Expanding views, *Neurosci. Biobehav. Rev.*, **59**(2015), 16–52.
3. D. Frosini, M. Cosottini, D. Volterrani, et al., Neuroimaging in Parkinson's disease: Focus on substantia nigra and nigro-striatal projection. *Curr. Opin. Neurol.*, **30**(2017), 416–426.
4. D. Berg, Ultrasound in the (premotor) diagnosis of Parkinson ' s disease, *Park. Relat. Disord.*, **13**(2007),13.
5. Q. Huang, F. Zhang and X. Li, Machine learning in ultrasound computer-aided diagnostic systems: A survey, *BioMed. Res. Int.*, 2018, Article ID: 5137904.
6. S. Zhou, J. Shi, J. Zhu, et al., Shearlet-based texture feature extraction for classification of breast tumor in ultrasound image, *Biomed. Signal Process. Control*, **8**(2013), 688–696.
7. G. Lehang, D. Wang, Y. Qian, et al., A two-stage multi-view learning framework based computer-aided diagnosis of liver tumors with contrast enhanced ultrasound images, *Clin. Hemorheol. Microcirc.*, **69**(2018), 343–354.
8. Q. Huang, Y. Chen, L. Liu, et al., On combining biclustering mining and AdaBoost for breast tumor classification, *IEEE Trans. Knowl. Data Eng.*, 2019, in press. DOI: 10.1109/TKDE.2019.2891622
9. L. Chen, J. Hagenah and A. Mertins, Feature analysis for Parkinson's disease detection based on transcranial sonography image, In *the 15th International Conference on Medical Image Computing and Computer-Assited Intervention*, 2012, 272–279.
10. O. Pauly, S. Ahmadi, A. Plate, et al., Detection of substantia nigra echogenicities in 3D transcranial ultrasound for early diagnosis of Parkinson disease, In *the 15th International Conference on Medical Image Computing and Computer-Assited Intervention*, 2012, 443–450.
11. A. Plate, S. Ahmadi, O. Pauly, et al., Three-dimensional sonographic examination of the midbrain for computer-aided diagnosis of movement disorders, *Ultrasound Med. Biol.*, **38**(2012), 2041–2050.
12. A. Sakalauskas, K. Laučkaitė, A. Lukoševičius, et al., Computer-aided segmentation of the mid-brain in trans-cranial ultrasound images, *Ultrasound Med. Biol.*, **42**(2016), 322–332.
13. A. Sakalauskas, V. Špečkauskienė, K. Laučkaitė, et al., A. Lukoševičius, Transcranial ultrasonographic image analysis system for decision support in Parkinson disease, *J. Ultrasound Med*., 2018.
14. B. Gong, J. Shi, S. Ying, et al., Neuroimaging-based diagnosis of Parkinson's disease with deep neural mapping large margin distribution machine, *Neurocomputing*, **320**(2018), 141–149.
15. J. Shi, Z. Y. Xue, Y. K. Dai, et al., Cascaded multi-column RVFL$^+$ classifier for single-modal neuroimaging-based diagnosis of Parkinson's disease, *IEEE Trans. Biomed. Eng.*, 2019, in press. DOI: 10.1109/TBME.2018.2889398.
16. K. Skerl, S. Vinnicombe, E. Giannotti, et al., Influence of region of interest size and ultrasound lesion size on the performance of 2D shear wave elastography (SWE) in solid breast masses, *Clin. Radiol.*, **70** (2015) 1421–1427.

17. J. Moon, J. Hwang, J. Park, et al., Impact of region of interest (ROI) size on the diagnostic performance of shear wave elastography in differentiating solid breast lesions, *Acta Radiol.*, **59** (2018), 657–663.
18. Q. Zhang, Y. Xiao, J. Suo, et al., Sonoelastomics for breast tumor classification: a radiomics approach with clustering-based feature selection on sonoelastography, *Ultrasound Med. Biol.*, **43** (2017), 1058–1069.
19. Y. Ma and L. Zhu, A review on dimension reduction, *Int. Statist. Rev.*, **81**(2013), 134–150.
20. J. Shi, Q. Jiang, Q. Zhang, et al., Sparse kernel entropy component analysis for dimensionality reduction of biomedical data, *Neurocomputing*, **168** (2015), 930–940.
21. J. Shi, Q. Jiang, R. Mao, et al., FR-KECA: Fuzzy robust kernel entropy component analysis, *Neurocomputing*, **149** (2015), 1415–1423.
22. B. Mwangi, T. Tian and J. Soares, A review of feature reduction techniques in neuroimaging, *Neuroinformatics*, **12** (2014), 229–244.
23. C. Ding and H. Peng, Minimum redundancy feature selection from microarray gene expression data, *J. Bioinform. Comput. Biol.*, **3**(2005), 185–205.

AIMS Press